Single laser source for multimodal coherent anti-Stokes Raman spectroscopy microscopy

Adrian F. Pegoraro,[1,2,*] Aaron D. Slepkov,[2] Andrew Ridsdale,[2] John Paul Pezacki,[2] and Albert Stolow[1,2]

[1]Department of Physics, Queen's University, Kingston, Ontario K7L 3N6, Canada

[2]Steacie Institute for Molecular Sciences, National Research Council of Canada, Ottawa, Ontario K1A 0R6, Canada

*Corresponding author: adrian.pegoraro@nrc-cnrc.gc.ca

Received 17 February 2010; revised 4 April 2010; accepted 26 April 2010; posted 4 May 2010 (Doc. ID 124348); published 0 MONTH 0000

Short laser pulse technology has significantly contributed to biomedical research, especially via nonlinear optical microscopy. Coherent anti-Stokes Raman spectroscopy (CARS) microscopy is a label-free, chemical-selective method that is growing in importance as improved methods and light sources develop. Here we discuss different approaches to laser source development for CARS microscopy and highlight the advantages of a multimodal CARS microscope, illustrated by selected applications in biomedical research. © 2010 Optical Society of America

OCIS codes: 170.5810, 180.4315, 300.6230.

1. Introduction

Laser use continues to make major inroads into biomedical research, with confocal laser scanning microscopy (CLSM) providing a prime example [1]. The most common CLSM systems use fluorescence for imaging, wherein the excitation wavelength is changed to measure different fluorescent dyes and molecules. The introduction of nonlinear optical (NLO) techniques has opened new doors for CLSM. For example, it has led both to new light sources for fluorescence microscopy [2] and to new techniques, such as stimulated emission depletion microscopy, to improve spatial resolution [3]. Pulsed lasers also enable new imaging modalities for CLSM. The most widely utilized NLO modality is two-photon fluorescence (TPF) imaging [4]. Other NLO techniques have also been used for imaging, such as second harmonic generation (SHG) [5] and third harmonic generation (THG) imaging [6]. NLO microscopy can allow contrast without requiring the addition of labels or dyes. Tissue samples, in particular, often demonstrate strong intrinsic nonlinear signals. In multimodal imaging, TPF, SHG, and THG make use of a single pump wavelength, using color filters to separate the signals; however, these do not demonstrate chemical specificity. For chemical specific imaging, confocal Raman is a well known technique, but it requires long acquisition times that are generally incompatible with live-cell microscopy. Coherent anti-Stokes Raman scattering (CARS) microscopy is a NLO imaging modality that overcomes this deficiency by using two lasers with their frequency difference tuned to a Raman vibrational resonance [7,8]. It is this driven (stimulated) aspect of CARS that leads to its greatly enhanced signal levels in comparison with spontaneous Raman scattering and enables faster imaging. By changing the wavelength of one or both lasers, different Raman resonances can be probed to better characterize the sample. CARS thus allows label-free, chemical-specific imaging and is becoming an important tool for the study of live samples. Here we discuss a simplified approach to

0003-6935/10/2500F1-01$15.00/0

multimodal CARS microscopy that we hope will encourage its expanded use in biomedical research.

Although CARS does offer significant advantages over other NLO modalities, there are also challenges that must be overcome for effective imaging, the most significant being the nonresonant background. The energy level diagrams for resonant and nonresonant CARS are illustrated in Fig. 1. We can see that both the resonant and the nonresonant components are indistinguishable by signal wavelength. Although this is not an issue for bulk samples composed only of resonant material, in microscopy, where the concentration of resonant molecules is small, this presents significant difficulties. There are many techniques that aim to overcome the nonresonant background and several review articles are available that highlight these [9–12]. The most common method of overcoming this problem is to use picosecond (ps) instead of femtosecond (fs) pulses to improve the contrast of resonant over nonresonant signals [13]. This has traditionally limited the choice of laser source commonly used for CARS microscopy to either two synchronized ps oscillators [14] or to a ps optical parametric oscillator (OPO) [15]. One drawback of this approach is that the use of ps pulses for CARS microscopy makes it more difficult to combine CARS with other NLO techniques in a multimodal microscope, since ultrashort (fs) pulsed lasers are the current tool of choice for NLO imaging. Although it is possible to acquire CARS and other NLO signals sequentially, ideally all signals should be acquired simultaneously. The question of which laser source to use, of course, depends on the application. The best solution for working in the fingerprint region (Raman shifts $<1700\,\mathrm{cm}^{-1}$) is not necessarily the best choice for lipid imaging (Raman shifts from 2700 to $3100\,\mathrm{cm}^{-1}$). To clarify this discussion, in Section 2 we show how the pulse spectral width is related to CARS microscopy performance, both in imaging and microspectroscopy applications. This highlights the need for flexible laser sources in multimodal CARS microscopy. We present a discussion of our simplified, fs-based approach to CARS microscopy that recently

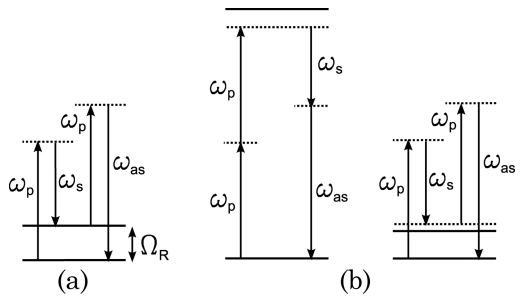

Fig. 1. (a) Energy level diagram for resonant CARS. The energy difference between pump ω_p and Stokes ω_s matches the energy of the Raman level to be probed Ω_R. The anti-Stokes ω_{as} light is the desired signal. (b) Energy level diagrams for nonresonant CARS. The anti-Stokes light generated has the same frequency as is generated in the resonant case, yet does not rely on ground-state vibrational coherence.

permitted commercialization of the first CARS microscope specifically designed for biomedical imaging of lipids [16].

2. Theory

Both ps and fs pulses can be used for CARS multimodal microscopy. The ideal laser for CARS microscopy depends on many factors, the most important one being the Raman vibration(s) probed. This is best illustrated with a simple model simulation, following the method of Cheng *et al.*[13]. Here we compare the performance of different pulse spectral widths for a given sample. The CARS polarization $P_{\mathrm{CARS}}(\omega_{as})$ is given by

$$P_{\mathrm{CARS}}(\omega_{as}) = \int_{-\infty}^{+\infty} \chi^{(3)} E_p(\omega_p) E_s^*(\omega_s) E_{pr}(\omega_{pr}) \mathrm{d}\omega, \quad (1)$$

where $E_p(\omega_p)$, $E_s(\omega_s)$, and $E_{pr}(\omega_{pr})$ are the electric fields of the pump, Stokes, and probe pulses, respectively. For degenerate CARS microscopy, the pump and probe are identical. The third-order susceptibility is given by $\chi^{(3)} = \chi_r^{(3)} + \chi_{nr}^{(3)}$, where $\chi_r^{(3)}$ and $\chi_{nr}^{(3)}$ denote the resonant and nonresonant susceptibilities, respectively. To model a single Raman resonance we use

$$\chi_r^{(3)} = \frac{A}{\Omega - (\omega_p - \omega_s) - i\Gamma}, \quad (2)$$

where Ω is the center frequency of the Raman mode, Γ is the linewidth, and A is a scale factor. The laser pulses are normalized to be of constant energy, regardless of spectral width. This choice of normalization has further implications when photodamage is taken into consideration, as discussed below:

$$E(t) = E\sqrt{\frac{\pi\delta}{2\ln 2}} \exp\left(\frac{-\pi^2\delta^2 t^2}{2\ln 2}\right) \exp(-i\omega t), \quad (3)$$

where E is amplitude, δ is the spectral width, and ω is the center frequency of the pulse.

To enable comparisons for practical imaging applications, we use parameters suitable for imaging lipids: a pump center frequency of $12500\,\mathrm{cm}^{-1}$ (800 nm) and a Stokes center frequency variable between 9575 and $9700\,\mathrm{cm}^{-1}$ (1030–1044 nm). The energy difference between the two pulses covers the 2800–$2925\,\mathrm{cm}^{-1}$ range. We use two overlapped resonant Raman modes to simulate a complex Raman structure. One mode has a Raman shift Ω_1 of $2850\,\mathrm{cm}^{-1}$ and a linewidth of $2\Gamma_1 = 15\,\mathrm{cm}^{-1}$; the other has a resonant frequency of Ω_2 of $2875\,\mathrm{cm}^{-1}$ and a Raman linewidth of $2\Gamma_2 = 20\,\mathrm{cm}^{-1}$. The mode centered at $2875\,\mathrm{cm}^{-1}$ is twice as strong as the one centered at $2850\,\mathrm{cm}^{-1}$ ($A_{2875} = 2A_{2850}$). The relative strength of the resonant to nonresonant signals modeled is $|A_{2850}/\chi_{nr}^{(3)}| = 0.01\,\mathrm{cm}^{-1}$ (this approximates the contrast achieved in practical systems [17]). For ease of comparison, the intensity

from the resonant and nonresonant contributions to $\chi^{(3)}$ is calculated separately.

In Fig. 2(a), the calculated resonant signals (intensity I_r) are shown as a function of Stokes center wavelength for different pulse durations. As expected, total signals increase and spectral resolution decreases as the spectral width of the pulses is increased (i.e., toward fs pulses). Figure 2(b) shows that the contrast (resonant divided by nonresonant intensity I_r/I_{nr}) improves with a smaller spectral width (i.e., toward ps pulses). This strongly suggests an advantage to the use of spectrally narrow pulses and is one of the primary reasons for choosing ps pulses; however, signal levels are also sacrificed with this choice. To characterize the compromise between contrast and desired resonant signal, we measure the performance $\mathbb{P}_f$, which is defined as the contrast multiplied by the resonant signal ($\mathbb{P}_f = I_r^2/I_{nr}$). The performance as a function of Stokes center wavelength for different pulse spectral widths is shown in Fig. 2(c).

Figure 2 illustrates some of the considerations for determining which pulse spectral width to use for a given sample. In this example, performance is maximized for pulses with a spectral width of $\sim$35 cm^{-1} and peaks at a frequency difference of $\sim$2870 cm^{-1}. If the combined Raman vibrations are approximated as a single Raman mode, this corresponds to the effective center frequency and Raman bandwidth. This demonstrates that for CARS imaging applications where it may not be critical to distinguish between adjacent Raman modes (e.g., lipid imaging in tissues), maximum performance is achieved by use of a pulse spectral width that matches the effective spectral width of the overlapped Raman modes, not the width of any particular band. For samples in which lipid imaging is used, this corresponds to pulses with a spectral width $>$100 cm^{-1} ($<$150 fs). On the other hand, if it is necessary to perform imaging while isolating a single Raman band, pulses that are spectrally narrow relative to the Raman resonance under observation are required, since they enable contrast between adjacent bands. This is particularly relevant in the fingerprint region in which there are many overlapped Raman bands with linewidths $<$10 cm^{-1} ($>$1.5 ps), which can produce a large nonresonant background when trying to image a specific band. This implies that a laser source with variable pulse spectral width is preferred for multimodal CARS imaging. The desire for flexibility in choosing the pulse spectral width is further reinforced when considering photodamage in NLO microscopy. If the mechanism of photodamage is a higher-order nonlinear process than the process that generates the signal, peak power could be used for normalization rather than constant energy as was employed above. In this case, to maintain a constant output signal, it would be preferable to use longer pulses with a higher average power. Eventually photodamage that is due to absorption in the sample would limit increasing the average power and thus set the optimal pulse duration. For TPF, the primary damage mechanism was found to scale linearly [18], quadratically [19], or faster than quadratically with intensity depending on the sample and laser used [20]. For CARS microscopy, photodamage has been shown to scale between linearly and quadratically with intensity depending on the sample and scanning conditions [21]. Consequently, peak power can be the sample-dependent limiting factor that favors longer pulses whereas the opposite is true when limited by average power. This again highlights the desire for flexibility in choosing the laser source used. Varying the pulse spectral width to either maximize performance or minimize photodamage can be accomplished by using multiple laser sources [22], using long doubling crystals to narrow the spectral bandwidth [23] or by temporally stretching (chirping) spectrally broad pulses to achieve an effectively narrower spectral bandwidth [17,24–27]. This last option is known as spectral focusing and allows the effective pulse spectral width at second order (the Raman resonance) to be continuously adjusted to the desired effective pulse bandwidth. This offers the further advantage that

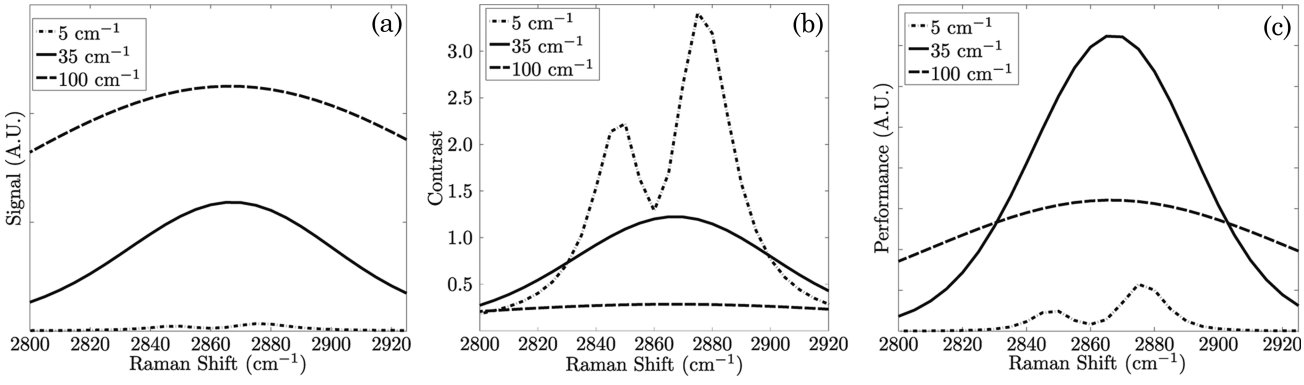

Fig. 2. The CARS (a) resonant signal, (b) contrast, and (c) performance are shown as a function of pump-Stokes frequency difference for varying pulse spectral widths for pulses of constant energy. The broadest (i.e., temporally shortest) pulse achieves the maximum resonant signal whereas maximum contrast is achieved for the narrowest (i.e., temporally longest) pulse. The individual peaks of the Raman spectrum are resolved only by use of the narrowest pulse. Performance is maximized for a pulse spectral width that matches the effective linewidth of the combined Raman mode; see text for definitions of contrast and performance.

optimization is performed after generation (i.e., it does not require modifying the laser) and is easily adjusted to suit a particular sample. Finally, this allows real-time feedback optimization of the CARS spectral resolution, image contrast, as well as signal strength from other NLO signals, as the effective pulse width is varied.

In microspectroscopy applications, it is the Raman spectrum of the sample that is measured. A straightforward approach to extracting the Raman spectrum using a CARS microscope is to use CARS imaging to locate points of interest in a sample and then to switch to confocal Raman microscopy to extract the spectral information [28]. This solution is particularly attractive for use in the fingerprint region, since it has been shown that confocal Raman offers comparable sensitivity to CARS in this region for live-cell microscopy applications [29]. If the CARS signal itself is used to extract spectral information, the procedure is more complex, but techniques are available. Multiplex CARS uses a ps pump and fs Stokes to probe many Raman modes simultaneously and the CARS spectrum is collected using a spectrometer [30,31]. Because of interference between the nonresonant background and the resonant signals, postprocessing of the CARS spectrum is required to extract the Raman spectrum [32]. More sophisticated techniques utilizing interference within fs pulses are also available [33,34]. A more direct approach is to record the CARS spectrum by varying the wavelength of one laser and reimaging the sample; however, interference with the nonresonant background causes the CARS and Raman spectra not to be identical. Either postprocessing or using interferometric techniques to retrieve the Raman spectrum can overcome this difficulty [35]. Regardless of the method used to extract the Raman spectrum, the effective pulse spectral width limits the achievable spectral resolution. It is worth noting that, when using chirped fs pulses, rather than changing the laser center wavelength it is possible to scan the frequency difference (i.e., the Raman resonance being probed) simply by changing the time delay between the pulses [17,26]. This is a simple way to perform spectral scans without adjusting the laser source and enables much faster spectral scanning. Again, the spectral resolution is optimized by changing the pulse chirp rate via dispersion engineering.

3. Toward All-Fiber Lasers

Regardless of the chosen pulse width, system stability and ease of use are primary concerns of microscopy end users. In CARS microscopes that use two synchronized lasers, timing jitter and alignment during spectral tuning are problematic and put additional constraints on the operating environment (temperature and vibrational stability) [14]. Use of an OPO to generate the pump and Stokes removes the problems with timing jitter and alignment during spectral tuning [15,27]. Use of a single laser and a photonic crystal fiber (PCF) to generate the Stokes, however, automatically synchronizes the pulses and represents a simple and cost-efficient method for performing CARS microscopy [17,36,37]. Laser alignment into the fiber is prone to vibrations and environmental changes, but automated fiber alignment feedback systems exist that can compensate for these drifts. These solutions rely on free-space lasers, whereas an all-fiber solution should offer improved stability and alleviate concerns about system alignment. It also offers a natural path to future integration with an endoscope for *in vivo* imaging. This was recognized early on in CARS microscopy and efforts were made to include fiber components for delivery of the excitation beams [38]. The main challenge using all-fiber generation for CARS microscopy is to generate a second, synchronized laser pulse at a different center wavelength. Replacing the pump laser with a fiber laser in an OPO apparatus is one approach to incorporating fiber lasers into CARS microscopy [39] but still requires generating the Stokes using free-space components.

Soliton shifting in highly nonlinear fibers plays a key role in generating the pulse pair in generation approaches [23,40,41]. Regardless of the nonlinear fiber used, the output pulses tend to be spectrally broad ($>200\ \mathrm{cm}^{-1}$) and must be accommodated if high spectral resolution is desired. Another concern is that the soliton generation process in fibers can be unstable unless the input pulse to the fiber is on the short fs time scale and transform limited [42,43]. This presents challenges for CARS microscopy where, in general, ps pulses have been preferred. One approach has been to design a system for multiplex CARS but to sacrifice rapid imaging, which is done with a ps fiber pump laser and then the use of two cascaded nonlinear fibers to first broaden then soliton shift the output to generate the Stokes pulse [40]. Use of a fs fiber laser alleviates the need to broaden the pulse before Stokes generation, but the resulting broad bandwidth pulse must be compensated by use of another technique if better spectral resolution is required for imaging. One method is to spectrally narrow both the pump and the Stokes by using long periodically poled doubling crystals [23]. On the other hand, use of spectral focusing to achieve the desired bandwidth offers the advantage of being able to easily tune the effective pulse spectral width while enabling other NLO microscopies by the short pulse [41]. Currently, all these approaches still use some free-space components and have relatively low power in comparison with existing free-space lasers; however, they present promising ideas for further development of stable, high average power, fiber laser sources for multimodal CARS microscopy.

4. Microscopy Setup

A depiction of a general CARS microscope optical arrangement is given in Fig. 3. A pump laser is combined with a method to generate the Stokes pulse. The Stokes can be generated by a second synchronized laser [14], an OPO [15,27], or a PCF [17,36,37]

as discussed above. The power utilized is limited by sample damage, with typical power levels of the order of 10–50 mW for live-cell imaging (assuming ~80 MHz pulse repetition rate and a pixel dwell time of ~4–8 μs). Integrated laser exposure time plays a significant role in determining cell damage, so increasing the microscope scan speed (i.e., reducing the pixel dwell time) allows for higher laser power at the sample [44]. Using wavelengths closer to the infrared also reduces sample damage [19]; however, water absorption sets an upper limit on the Stokes wavelength (at ~1.5 μm). Longer wavelengths also offer the added advantage of reducing scattering losses that enable greater penetration depth into samples. This has been most successfully demonstrated with ps OPOs with a degeneracy point at 1.05 μm, which provides pump and Stokes wavelengths at ~900 and 1260 nm, respectively; however, if comparable fs sources are developed, they should provide the same benefits. The microscope used for CARS imaging can vary considerably depending on the application. Most systems make use of objectives with a high numerical aperture (NA) that allow the pump and Stokes to be sent into the microscope collinearly. Tight focusing relaxes the phase-matching condition typically requisite for a four-wave mixing process such as CARS. The CARS signal is much stronger in the forward direction, and this is often used if the sample permits it [13] . For thick tissue samples and live animal studies, the signal must of course be collected in the epidirection. For multimodal imaging, the different signals are separated by use of dichroic beam splitters and filters.

5. Applications

Here we present applications of multimodal CARS microscopy, including those based on the simplified approach highlighted in this article. Much of the interest in optimizing the source for multimodal CARS microscopy derives from the advantages it offers for the study of live cells and tissue. Although CARS can be used to image different Raman modes (e.g., D_2O to study water dynamics [45]), most applications focus on lipid imaging using CARS, due to its strong,

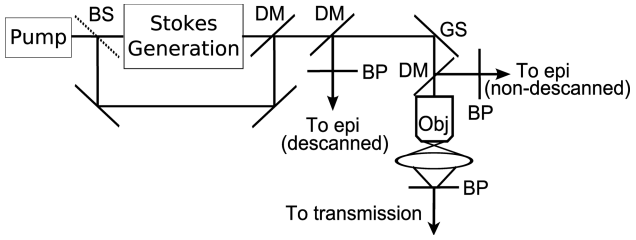

Fig. 3. Generalized CARS microscopy optical setup. The pump laser is split using a beam splitter (BS). Part of the beam is used to generate a Stokes pulse; the other part is delayed then recombined and overlapped with the Stokes on a dichroic mirror (DM). Inside the microscope galvo-scanning mirrors (GS) direct the beam. Dichroic mirrors and bandpass (BP) filters separate the signals from the excitation light. Epidetected signals can be collected before or after the galvo mirrors (descanned or nondescanned detection).

relatively isolated Raman band and high concentration of oscillators. When complemented with other microscopies, CARS imaging provides new information about the sample. One technique that can be advantageously combined with CARS is differential interference contrast (DIC), which offers label-free images primarily based on density changes in the sample. DIC can be enhanced by using CARS to highlight objects of interest based on their Raman signature [46]. Because DIC is a low power technique, this allows rapid imaging over long time periods without fear of cellular damage. We, for example, used this combination to study the effects of the Hepatitis C virus (HCV) on liver cells. HCV is known to cause lipid drop accumulation [47,48]; to study these changes CARS is used to locate lipid drops whereas DIC is used to track them. An example showing a CARS image taken using chirped fs pulses overlaid on DIC is shown in Fig. 4(a). CARS can also be combined with traditional fluorescent labeling techniques to offer enhanced information. If CARS and TPF are measured using the same laser, it ensures that the signals are coregistered and allows for collocalization studies. This has been used to study several different problems in cellular dynamics. Figure 4(b) again highlights the use of CARS to study HCV. Here, the HCV construct has been modified to induce the production of green fluorescent protein (GFP). TPF is used to identify infected cells, and CARS is used to track lipid movement and accumulation. Chirped fs pulses are used to collect both signals simultaneously.

Tissue samples offer another area in which multimodal NLO microscopy provides significant advantages. Although fluorescent staining can be employed, many samples demonstrate endogenous fluorescence that obviates the need for labeling.

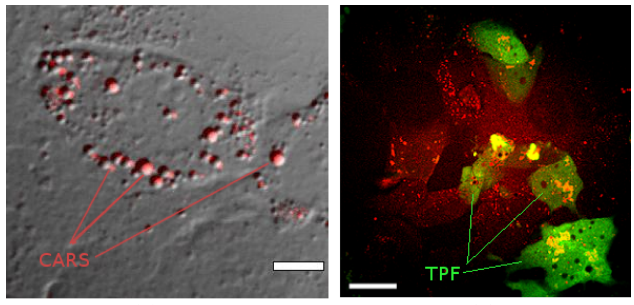

Fig. 4. (Color online) (a) CARS and DIC multimodal imaging of HuH-7 liver cells. The CARS image was taken first using chirped fs pulses and then overlapped with a subsequent DIC image. In print, some of the lipid drops are indicated; online, red represents CARS due to lipids, gray represents the DIC image. Scale bar is 5 μm. (b) CARS and TPF multimodal image of HuH-7 cells infected with a modified HCV strain (infected cells express GFP). The images were acquired simultaneously using chirped fs pulses as part of a time course studying live cells (taken at the 48 h time point). In print, the areas indicated are TPF due to GFP; the remainder of the image is CARS due to lipids. Online, greenrepresents TPF due to GFP; red represents CARS due to lipids. Scale bar is 10 μm.

Furthermore, the long-range structure present in tissues allows SHG to be used as a third contrast mechanism. Sum frequency generation and THG can also be used, offering additional tools for the study of samples. Of particular interest is combining CARS, SHG and TPF since all three signals can be collected using the same lasers and are often spectrally distinct. This has been demonstrated for the study of atherosclerotic plaque in which all three signals have endogenous sources [22]. An example image taken using chirped pulses is shown in Fig. 5(a), where the blue is due to SHG from collagen that composes the cap of the arterial plaque, green is TPF from elastin in the artery wall, and red is CARS from lipids located inside the plaque. This particular sample is from a Watanabe heritable hyperlipidemic myocardial infarction (WHHLMI) rabbit strain [49] where the disease progression is well known. By characterizing plaques using traditional techniques as well as NLO microscopy, it is hoped to design methods of diagnosing plaque severity *in vivo*. Thin tissue samples offer the additional advantage of allowing collection in both the forward and the backward direction, which enables studying the ratio of a forward to backward collected signal to better characterize tissue composition. This is important in understanding disease as well as basic tissue morphology. For example, by using SHG, CARS, and THG, it has been demonstrated that ordering in tissue can be characterized as the techniques are sensitive to different heterogeneities [50]. For example, SHG [Fig. 5(b)], CARS [Fig. 5(c)], and THG [Fig. 5(d)] all reveal different information about fascia samples (TPF and THG taken using fs pulses, CARS using ps pulses). Although SHG measures the heterogeneity of $\chi^{(2)}$, THG is used to measure interfaces between collagen sheets and CARS is used to measure bulk structure. The results suggest that SHG in collagen is due to imperfect cancellation rather than from individual collagen fibrils, since THG and CARS do not indicate the same level of heterogeneity.

Multimodal NLO microscopy also applies to live tissue imaging in which endogenous signals can be utilized without damaging the sample. The two main alterations from working with cells and thin tissue samples are that all the signals must be collected

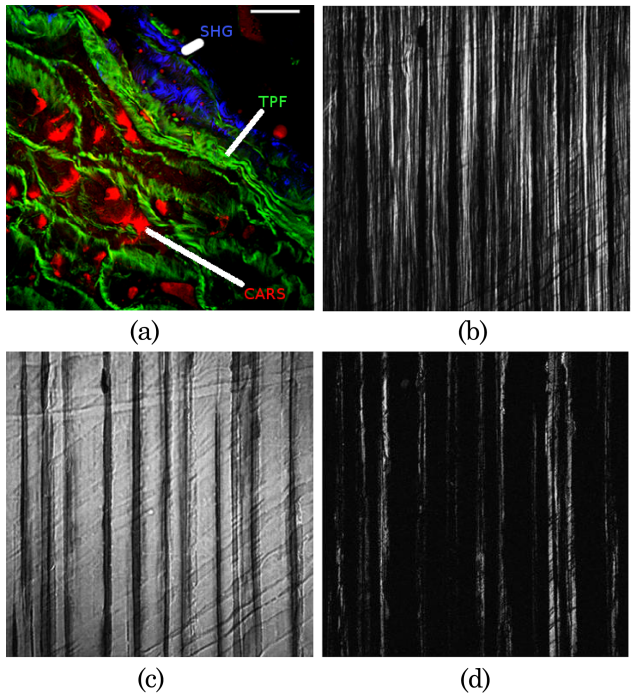

Fig. 5. (Color online) (a) WHHMLI arterial sample. Online, red represents CARS imaging of lipids, green represents TPF from elastin, and blue represents SHG from collagen. In print, the different parts of the sample are labeled. All the signals were collected simultaneously using chirped fs pulses. Scale bar is 50 μm. Multimodal nonlinear optical imaging of fascia. (b) Forward SHG image using fs pulses, (c) forward CARS image at Raman shift frequency $\Delta\omega = 2845\,\mathrm{cm}^{-1}$ using ps pulses, and (d) forward THG image using fs pulses. Scanning area was $146.2\,\mu\mathrm{m}^2$ (512×512 pixels). (b), (c) and (d) reprinted with permission from [50].

in the epidirection and that long working distance microscope objectives are preferred. Both CARS and SHG are emitted in the epidirection if the particles of interest are subwavelength; however, the forward propagating signal also rescatters in the backward direction and represents the majority of the signal collected [44,51]. Given the large lipid content in myelin, CARS has been particularly successful in studying nerve damage and recovery [52–54]. When imaging in live animals, longitudinal studies are possible to better understand damage to the spine, coping mechanisms, and long-term recovery. Another

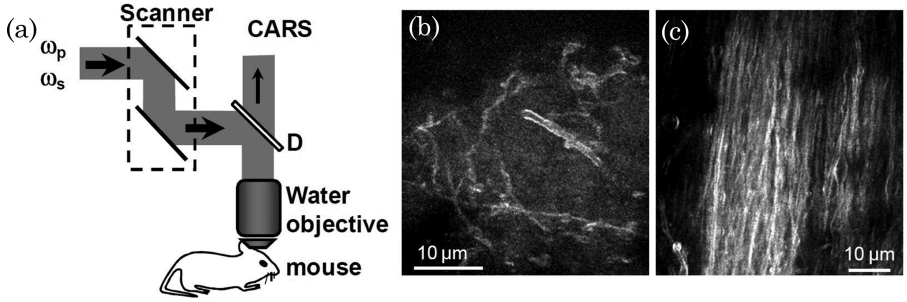

Fig. 6. *In vivo* CARS imaging using ps pulses of mouse brain using an upright microscope with a dipping mode water objective. (a) A schematic of the *in vivo* CARS microscope; D, dichroic mirror. (b) CARS image of the parietal cortex. (c) Epi-CARS image of bundles of myelinated fibers in the subcortex white matter. Reprinted with permission from [52].

example is to use CARS to study white matter in the brain, as shown in Fig. 6 (ps pulses were used) [52]. Currently, most live tissue work makes use of microsurgery to expose the area of interest, highlighting the need for endoscopic options for multimodal microscopy to increase its utility and versatility.

While most applications of CARS microscopy have focused on imaging a single Raman resonance, extracting spectral information is used in some applications. For example, multiplex CARS has been used to study the effects of temperature change on lipid domains [32]. CARS combined with confocal Raman has been used to study the differences between lipid droplets in live animal versus cell culture models, important for understanding and validating cell models [28]. This could be used, for example, to study the effect of different obesity treatments from drug use to the effects of dietary changes.

6. Conclusion and Outlook

Laser technology now plays a key role in biomedical research, and we believe that multimodal NLO optical microscopy, in particular, will continue to play an expanding role in the life sciences. Label-free techniques are particularly important for studying live samples in both cells and animal models. CARS microscopy offers a new label-free modality that plays an increasingly important role in multimodal microscopy. Development in laser sources will be a key enabling technology for the spread of this technique. Fiber lasers will likely play an increasingly important role in NLO microscopy, enabling use in a wider variety of settings. Using fiber lasers will also make coupling to endoscopes substantially easier, which will be necessary if NLO microscopy is to be used for patient diagnostics (beyond the skin and eye) without requiring surgery for imaging. Existing sources, however, already allow effective multimodal CARS microscopy for biomedical research. As we have shown here, simplified sources that offer the user control over the effective pulse spectral bandwidth are versatile for multimodal NLO microscopy. Recently, this approach was successfully implemented by a major microscope manufacturer (Olympus America) to produce the world's first commercially available CARS microscope [16]. These developments along with the work of many other research groups will continue to make multimodal CARS microscopy available to study a wide variety of problems in biomedical research.

The assistance of Rodney Lyn for the HuH-7 cells and Alex Ko at the Institute for Biodiagnostics, National Research Council of Canada, Winnipeg, Manitoba, Canada, for rabbit artery samples are gratefully acknowledged. A. Pegoraro thanks the National Sciences and Engineering Research Council of Canada (NSERC) and the National Research Council of Canada (NRC) for funding support.

References

1. J. B. Pawley, ed., *Handbook of Biological Confocal Microscopy* (Springer, 2006).
2. T. Betz, J. Teipel, D. Koch, W. Hartig, J. Guck, J. Kas, and H. Giessen, "Excitation beyond the monochromatic laser limit: simultaneous 3-D confocal and multiphoton microscopy with a tapered fiber as white-light laser source," J. Biomed. Opt. **10**, 054009 (2005).
3. S. W. Hell and J. Wichmann, "Breaking the diffraction resolution limit by stimulated emission: stimulated-emission-depletion fluorescence microscopy," Opt. Lett. **19**, 780–782 (1994).
4. W. Denk, J. Strickler, and W. Webb, "Two-photon laser scanning fluorescence microscopy," Science **248**, 73–76 (1990).
5. P. J. Campagnola, M.-d. Wei, A. Lewis, and L. M. Loew, "High-resolution nonlinear optical imaging of live cells by second harmonic generation," Biophys. J. **77**, 3341–3349 (1999).
6. D. Yelin and Y. Silberberg, "Laser scanning third-harmonic-generation microscopy in biology," Opt. Express **5**, 169–175 (1999).
7. M. D. Duncan, J. Reintjes, and T. J. Manuccia, "Scanning coherent anti-Stokes Raman microscope," Opt. Lett. **7**, 350–352 (1982).
8. A. Zumbusch, G. R. Holtom, and X. S. Xie, "Three-dimensional vibrational imaging by coherent anti-Stokes Raman scattering," Phys. Rev. Lett. **82**, 4142–4145 (1999).
9. J.-X. Cheng and X. Xie, "Coherent anti-Stokes Raman scattering microscopy: instrumentation, theory, and applications," J. Phys. Chem. B **108**, 827–840 (2004).
10. A. Volkmer, "Vibrational imaging and microspectroscopies based on coherent anti-Stokes Raman scattering microscopy," J. Phys. D **38**, R59–R81 (2005).
11. J.-X. Cheng, "Coherent anti-Stokes Raman scattering microscopy," Appl. Spectrosc. **61**, 197–208 (2007).
12. C. L. Evans and X. S. Xie, "Coherent anti-Stokes Raman scattering microscopy: chemical imaging for biology and medicine," Annu. Rev. Anal. Chem. **1**, 883–909 (2008).
13. J.-x. Cheng, A. Volkmer, L. Book, and X. Xie, "An epi-detected coherent anti-Stokes Raman scattering (*E*-CARS) microscope with high spectral resolution and high sensitivity," J. Phys. Chem. B **105**, 1277–1280 (2001).
14. D. J. Jones, E. O. Potma, J.-X. Cheng, B. Burfeindt, Y. Pang, J. Ye, and X. S. Xie, "Synchronization of two passively mode-locked, picosecond lasers within 20 fs for coherent anti-Stokes Raman scattering microscopy," Rev. Sci. Instrum. **73**, 2843–2848 (2002).
15. F. Ganikhanov, S. Carrasco, X. S. Xie, M. Katz, W. Seitz, and D. Kopf, "Broadly tunable dual-wavelength light source for coherent anti-Stokes Raman scattering microscopy," Opt. Lett. **31**, 1292–1294 (2006).
16. "Fluoview FV1000MPE femtocars add-on," http://www.olympusamerica.com/seg_section/product.asp?product=1068&intCmp=seg_rdct_cars (2010).
17. A. F. Pegoraro, A. Ridsdale, D. J. Moffatt, Y. Jia, J. P. Pezacki, and A. Stolow, "Optimally chirped multimodal CARS microscopy based on a single Ti:sapphire oscillator," Opt. Express **17**, 2984–2996 (2009).
18. B. R. Masters, P. T. C. So, C. Buehler, N. Barry, J. D. Sutin, W. W. Mantulin, and E. Gratton, "Mitigating thermal mechanical damage potential during two-photon dermal imaging," J. Biomed. Opt. **9**, 1265–1270 (2004).
19. K. König, T. W. Becker, P. Fischer, I. Riemann, and K.-J. Halbhuber, "Pulse-length dependence of cellular response to intense near-infrared laser pulses in multiphoton microscopes," Opt. Lett. **24**, 113–115 (1999).
20. A. Hopt and E. Neher, "Highly nonlinear photodamage in two-photon fluorescence microscopy," Biophys. J. **80**, 2029–2036 (2001).
21. Y. Fu, H. Wang, R. Shi, and J.-X. Cheng, "Characterization of photodamage in coherent anti-Stokes Raman scattering microscopy," Opt. Express **14**, 3942–3951 (2006).
22. T. T. Le, I. M. Langohr, M. J. Locker, M. Sturek, and J.-X. Cheng, "Label-free molecular imaging of atherosclerotic

lesions using multimodal nonlinear optical microscopy," J. Biomed. Opt. **12**, 054007 (2007).
23. G. Krauss, T. Hanke, A. Sell, D. Träutlein, A. Leitenstorfer, R. Selm, M. Winterhalder, and A. Zumbusch, "Compact coherent anti-Stokes Raman scattering microscope based on a picosecond two-color Er:fiber laser system," Opt. Lett. **34**, 2847–2849 (2009).
24. E. T. J. Nibbering, D. A. Wiersma, and K. Duppen, "Ultrafast nonlinear spectroscopy with chirped optical pulses," Phys. Rev. Lett. **68**, 514–517 (1992).
25. K. Duppen, F. de Haan, E. T. J. Nibbering, and D. A. Wiersma, "Chirped four-wave mixing," Phys. Rev. A **47**, 5120–5137 (1993).
26. T. Hellerer, A. M. Enejder, and A. Zumbusch, "Spectral focusing: high spectral resolution spectroscopy with broadbandwidth laser pulses," Appl. Phys. Lett. **85**, 25–27 (2004).
27. I. Rocha-Mendoza, W. Langbein, and P. Borri, "Coherent anti-Stokes Raman microspectroscopy using spectral focusing with glass dispersion," Appl. Phys. Lett. **93**, 201103 (2008).
28. M. N. Slipchenko, T. T. Le, H. Chen, and J.-X. Cheng, "High-speed vibrational imaging and spectral analysis of lipid bodies by compound Raman microscopy," J. Phys. Chem. B **113**, 7681–7686 (2009).
29. M. Cui, B. R. Bachler, and J. P. Ogilvie, "Comparing coherent and spontaneous Raman scattering under biological imaging conditions," Opt. Lett. **34**, 773–775 (2009).
30. M. Muller and J. M. Schins, "Imaging the thermodynamic state of lipid membranes with multiplex CARS microscopy," J. Phys. Chem. B **106**, 3715–3723 (2002).
31. J. Cheng, A. Volkmer, L. D. Book, and X. S. Xie, "Multiplex coherent anti-Stokes Raman scattering microspectroscopy and study of lipid vesicles," J. Phys. Chem. B **106**, 8493–8498 (2002).
32. H. A. Rinia, M. Bonn, M. Müller, and E. M. Vartiainen, "Quantitative CARS spectroscopy using the maximum entropy method: the main lipid phase transition," Chem. PhysChem. **8**, 279–287 (2007).
33. N. Dudovich, D. Oron, and Y. Silberberg, "Single-pulse coherently controlled nonlinear Raman spectroscopy and microscopy," Nature **418**, 512–514 (2002).
34. J. P. Ogilvie, E. Beaurepaire, A. Alexandrou, and M. Joffre, "Fourier-transform coherent anti-Stokes Raman scattering microscopy," Opt. Lett. **31**, 480–482 (2006).
35. E. O. Potma, C. L. Evans, and X. S. Xie, "Heterodyne coherent anti-Stokes Raman scattering (CARS) imaging," Opt. Lett. **31**, 241–243 (2006).
36. E. R. Andresen, H. N. Paulsen, V. Birkedal, J. Thøgersen, and S. R. Keiding, "Broadband multiplex coherent anti-Stokes Raman scattering microscopy employing photonic-crystal fibers," J. Opt. Soc. Am. B **22**, 1934–1938 (2005).
37. E. R. Andresen, V. Birkedal, J. Thøgersen, and S. R. Keiding, "Tunable light source for coherent anti-Stokes Raman scattering microspectroscopy based on the soliton self-frequency shift," Opt. Lett. **31**, 1328–1330 (2006).
38. F. Légaré, C. L. Evans, F. Ganikhanov, and X. S. Xie, "Towards CARS endoscopy," Opt. Express **14**, 4427–4432 (2006).
39. K. Kieu, B. G. Saar, G. R. Holtom, X. S. Xie, and F. W. Wise, "High-power picosecond fiber source for coherent Raman microscopy," Opt. Lett. **34**, 2051–2053 (2009).
40. E. R. Andresen, C. K. Nielsen, J. Thøgersen, and S. R. Keiding, "Fiber laser-based light source for coherent anti-Stokes Raman scattering microspectroscopy," Opt. Express **15**, 4848–4856 (2007).
41. A. F. Pegoraro, A. Ridsdale, D. J. Moffatt, J. P. Pezacki, B. K. Thomas, L. Fu, L. Dong, M. E. Fermann, and A. Stolow, "All-fiber CARS microscopy of live cells," Opt. Express **17**, 20700–20706 (2009).
42. K. L. Corwin, N. R. Newbury, J. M. Dudley, S. Coen, S. A. Diddams, K. Weber, and R. S. Windeler, "Fundamental noise limitations to supercontinuum generation in microstructure fiber," Phys. Rev. Lett. **90**, 113904 (2003).
43. K. L. Corwin, N. R. Newbury, J. M. Dudley, S. Coen, S. A. Diddams, B. R. Washburn, K. Weber, and R. S. Windeller, "Fundamental amplitude noise limitations to supercontinuum spectra generated in a microstructured fiber," Appl. Phys. B **77**, 269–277 (2003).
44. C. L. Evans, E. O. Potma, M. Puoris'haag, D. Cote, C. P. Lin, and X. S. Xie, "Chemical imaging of tissue in vivo with videorate coherent anti-Stokes Raman scattering microscopy," Proc. Natl. Acad. Sci. USA **102**, 16807–16812 (2005).
45. E. O. Potma, W. P. de Boeij, P. J. M. van Haastert, and D. A. Wiersma, "Real-time visualization of intracellular hydrodynamics in single living cells," Proc. Natl. Acad. Sci. USA **98**, 1577–1582 (2001).
46. J.-X. Cheng, Y. K. Jia, G. Zheng, and X. S. Xie, "Laser-scanning coherent anti-Stokes Raman scattering microscopy and applications to cell biology," Biophys. J. **83**, 502–509 (2002).
47. X. Nan, A. M. Tonary, A. Stolow, X. S. Xie, and J. P. Pezacki, "Intracellular imaging of HCV RNA and cellular lipids by using simultaneous two-photon fluorescence and coherent anti-Stokes Raman scattering microscopies," ChemBioChem **7**, 1895–1897 (2006).
48. R. K. Lyn, D. C. Kennedy, S. M. Sagan, D. R. Blais, Y. Rouleau, A. F. Pegoraro, X. S. Xie, A. Stolow, and J. P. Pezacki, "Direct imaging of the disruption of hepatitis c virus replication complexes by inhibitors of lipid metabolism," Virology **394**, 130–142 (2009).
49. M. Shiomi, T. Ito, S. Yamada, S. Kawashima, and J. Fan, "Development of an animal model for spontaneous myocardial infarction (WHHLMI Rabbit)," Arterioscler. Thromb. Vasc. Biol. **23**, 1239–1244 (2003).
50. C. P. Pfeffer, B. R. Olsen, F. Ganikhanov, and F. Légaré, "Multimodal nonlinear optical imaging of collagen arrays," J. Struct. Biol. **164**, 140–145 (2008).
51. F. Légaré, C. Pfeffer, and B. R. Olsen, "The role of backscattering in SHG tissue imaging," Biophys. J. **93**, 1312–1320 (2007).
52. Y. Fu, T. B. Huff, H.-W. Wang, J.-X. Cheng, and H. Wang, "Ex vivo and in vivo imaging of myelin fibers in mouse brain by coherent anti-Stokes Raman scattering microscopy," Opt. Express **16**, 19396–19409 (2008).
53. E. Bélanger, S. Bégin, S. Laffray, Y. D. Koninck, R. Vallée, and D. Côté, "Quantitative myelin imaging with coherent anti-Stokes Raman scattering microscopy: alleviating the excitation polarization dependence with circularly polarized laser beams," Opt. Express **17**, 18419–18432 (2009).
54. F. P. Henry, D. Côté, M. A. Randolph, E. A. Z. Rust, R. W. Redmond, I. E. Kochevar, C. P. Lin, and J. M. Winograd, "Real-time in vivo assessment of the nerve microenvironment with coherent anti-Stokes Raman scattering microscopy," Plast. Reconstr. Surg. **123**, 123S–130S (2009).